Inorganic Chemistry

Article

pubs.acs.org/IC

Multifaceted Approach for the Fabrication of Metallomicelles and Metallic Nanoparticles Using Solvophobic Bisdodecylaminepalladium (II) Chloride as Precursor

Ganga Ram Chaudhary,*[,†] Prabjot Singh,[†] Gurpreet Kaur,[†] S.K. Mehta,[†] Sandeep Kumar,[‡] and Neeraj Dilbaghi[‡]

[†]Department of Chemistry and Centre of Advanced Studies in Chemistry, Panjab University, Chandigarh 160 014, India

[‡]Department of Bio and Nano Technology, Guru Jambheshwar University of Science & Technology, Hisar 125 001, Haryana India

Supporting Information

ABSTRACT: A one-pot synthesis of solvophobic bisdodecylaminepalladium-(II) chloride (**complex 1**) was performed. **Complex 1** was characterized using X-ray crystallography and other techniques, namely, mass spectrometry, Fourier transform infrared, NMR, elemental analysis, etc. A multifaceted approach was taken to explore the potential applications of **complex 1**. The micellization ability of **complex 1** was estimated using conductivity method in *n*-alcohols. The metallomicelles are formed in alcohols, and the process is thermodynamically spontaneous in nature. Using **complex 1** as precursor, palladium (Pd) nanoparticles were fabricated using two-phase redox method, where reduction is being performed in core of metallomicelles formed by **complex 1** in dichloromethane (DCM). The micellization in DCM is confirmed by small-angle X-ray scattering (SAXS). The SAXS measurements reveal that the micellar of core 4−5 nm is being formed, which further controls the size of nanoparticle. This approach was advantageous in terms of size control, methodology, and yield. Pd nanoparticles were characterized using transmission electron microscopy, energy-dispersive X-ray spectroscopy, X-ray diffraction, and UV−visible spectroscopy and were also screened for bovine serum albumin interactions. **Complex 1** and Pd nanoparticles were found to possess antimicrobial property with broad spectrum and are active against bacteria and fungi. The cytotoxicity analyses were performed over healthy cells (Vero cell lines extracted from kidney of green monkey), and the results reveal IC_{50} value of 10 μg/mL for **complex 1**.

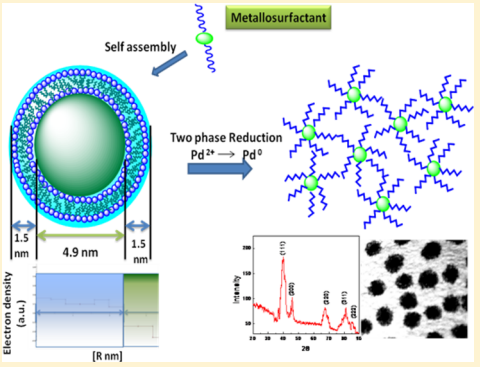

INTRODUCTION

Metal complexes are known for years now, and because of their redox properties and rich coordination chemistry, they have found applications in diverse areas such as synthetic enzymes, foot printing agents, spectroscopic probes, and molecular photoswitches.[1−3] A number of biochemical/biophysical processes make use of these biogenic metal cations like Na^+, K^+, Mg^{2+}, Ca^{2+}, Zn^{2+}, Mn^{2+}, $Fe^{2+/3+}$, $Co^{2+/3+}$, Ni^{2+}, and $Cu^{+/2+}$.[4] Among many, platinum-based drug cisplatin has come a long way because platinum(II) anticancer complexes form coordinate bonds with their target DNA. At the same time, metal complexes bearing ethylenediamine have also been of interest because in the classical antitumor agent cisplatin, N-donor is one of the ligands and possesses at least one hydrogen atom attached to the nitrogen.[5] Among various metal ions available, we selected palladium for the synthesis of double-chained diamine complex due to the extraordinary properties of its amphiphilic alkyl complexes, as enhanced catalytic agents,[6−9] application of metallic nanoparticles (NPs) in various fields,[10] as efficient drug delivery systems,[11] thin film devices,[12] etc.

The success of metallopharmaceutics has raised interest of many researchers to focus on metalloaggregates formed from so-called metallosurfactants. Metallosurfactants are special kind of amphiphilic complexes, where d or f block metal ions are complexed to surfactant molecules having one or more donor atoms. They find applications in many fields such as catalysis,[13] apoptosis-induction studies in cancer cells,[14] formation of lamellar superstructures,[15] DNA templates,[16] templates for metallic mesostructures,[17] etc. Valls et al.[18] have synthesized, isolated, and characterized metallosurfactants of palladium using amphiphilic alkylphosphines as ligands and studied their aggregation behavior, which is quite interesting due to presence of metal ion. Metallosurfactants aggregate to form metallomicelles,[19,20] metallovesicles[21−24] including small unilamellar vesicles (size 30−50 nm) and large unilamellar vesicles (size 100−200 nm), and multilamellar vesicles (onionlike packing of bilayers). The encouraging results provoked us to study their aggregation for utilizing them as vectors in different fields like gene delivery, targeted drug delivery, nano reactors, etc.

Various methods have been reported in literature for the synthesis of Pd NPs,[25−27] but metallosurfactants offer better

Received: May 23, 2015
Published: September 11, 2015

DOI: 10.1021/acs.inorgchem.5b01171
Inorg. Chem. 2015, 54, 9002−9012

routes. This is because of the following advantages: (i) smaller and narrow range of particle size distribution with greater degree of uniformity, (ii) high yields as only ligand-protected NPs remain in organic phase and rest of byproducts pass on to aqueous phase, (iii) no requirement of external stabilizing agents, as are used by other methods to avoid aggregation of NPs, (iv) cost-effective, since many methods reported in literature make use of costly chemicals like ionic liquids,[28] dendrimers,[29] beta zeolites,[30] etc., (v) comparatively simple method and does not involve complicated ligand syntheses, (vi) less time-consuming. Wang et al.[31] have reported in situ generation of metallosurfactants of palladium followed by the formation of metallic palladium NPs, which have been utilized in catalyzing Mizoroki Heck reaction. Of many catalytic systems of palladium,[32,33] metallic NPs of palladium are of great significance and are widely used to convert various substrates efficiently into desired products with remarkable yields.[34,35]

Owing to high adsorption tendency, conventional surfactants are also known for antimicrobial activity.[36,37] Therefore, we have made an attempt to compare the antimicrobial activity of conventional surfactant with that of metallosurfactant. In a report by Kumar and Arunachalam,[38] the antimicrobial activity of some cobalt metallosurfactants was evaluated against certain pathogenic microbes. Moreover, knowing antimicrobial activity and biocompatibility of metallosurfactants, these can be integrated into systems relevant for pharmaceutical industry, biomedical, and biosensing applications.

In present investigation, we report one-pot synthesis of a novel double-chained metallocomplex bisdodecylamine-palladium(II) chloride $[Pd(C_{12}H_{25}NH_2)_2]Cl_2$ (**complex 1**) by ligand-insertion method. The idea is to explore the aggregation behavior of metal complex containing dodecylamine chains. **Complex 1** was isolated and evaluated for its structural details using X-ray crystallography, elemental analyses, Fourier transform infrared (FTIR), mass spectrometry (MS), and thermogravimetric analysis (TGA). Further, the self-aggregation behavior was analyzed along with the estimation of thermodynamics of micellization using conductivity, dynamic light scattering (DLS), and small-angle X-ray spectroscopy (SAXS). An attempt was made to synthesize palladium NPs using **complex 1** as precursor by employing two phase (water/dichloromethane (DCM)) redox method. Synthesized NPs were characterized with transmission electron microscopy (TEM), DLS energy-dispersive X-ray spectroscopy (EDX), and X-ray diffraction. NPs were also evaluated for their interactions with bovine serum albumin (BSA) protein. Further, cytotoxicity of **complex 1** was evaluated toward healthy Vero cell lines and antimicrobial profile toward microorganisms (bacteria and fungus).

EXPERIMENTAL SECTION

Chemicals. Palladium(II) chloride (99%), dodecylamine (98.6%), tetramethylsilane (99.4%), Minimum Essential Medium Eagle (MEM) media containing 5% foetal bovine serum (FBS), BSA (98%), ceftriaxone, and $CDCl_3$ (99.2%) were purchased from Sigma-Aldrich. Sodium borohydride (95.4%) was purchased from Merck. Dimethylformamide (DMF) was dried with matrix molecular sieves 5Å, 30−40 mesh supplied by Sigma-Aldrich. Absolute ethanol (99.9%) was purchased from Changshu Yuang. DCM (99.5%) was purchased from Fisher Scientific. Phosphate buffer saline (99.3%) powder was purchased from Merck. Resazurin sodium, nutrient agar, and potato dextrose agar were purchased from HiMedia, Mumbai, India. Bacteria and fungi were procured from Indian-type culture collection, Indian agriculture research institute (IARI), New Delhi. Water was doubly distilled prior to use. All glassware and magnetic beads were cleaned with aqua regia followed by multiple rinses with doubly distilled water. There are no significant hazards associated with the reported experimental work. However, DCM and DMF were used; therefore, their safety data sheets were consulted.

Physical Measurements. C, H, N analyses of the synthesized bisdodecylaminepalladium(II) chloride (**complex 1**) was performed by PerkinElmer 2400 CHN/analytischer Vario EL II Fab. Nr. 11975059. All the CHN experiments were performed under nitrogen. Infrared spectroscopic studies were performed using PerkinElmer-FTIR Spectrum-100 operated in the spectral domain of 400−4000 cm^{-1} at a resolution of 4 cm^{-1}. KBr pellets were used to hold the sample, and 32 scans were taken for statistical averaging. For ^1H NMR studies, JEOL FT NMR, AL 300 was employed with 300 MHz radio frequency and 7.05 T magnetic field strength. Tetramethylsilane was used as internal standard, and deuterated chloroform was used as solvent. Micromass ES-MS, Q-TOF operated at 70 eV was used for mass spectrometry. Electron impact beam (EIB) was used as ionizing medium. Single-crystal X-ray studies were performed by using Bruker AXS, consisting of four axis κ goniometer module with an APEX II CCD detector. The crystals were positioned 40 mm from the CCD, and the diffraction spots were measured using a counting time of 10 s. The structure was solved and refined using the Bruker SHELXTL Software Package. Anisotropic thermal parameters were used for all non-H atoms. The hydrogen atoms of C−H groups were with isotropic parameters equivalent to 1.2 times those of the atom to which they were attached. All other calculations were performed using the program WinGX17. For TGA, Universal T.A. SDT Q-600 V 20.9 was used, where change in mass was noted with rise in temperature at a rate of 5 °C/min using standard alumina pans. Conductivity measurements were performed with Pico Conductivity meter (from Lab India; cell constant = 0.987 cm^{-1}). The glass cell was connected to the RE 320 Ecoline thermostat controlled to better than ±0.01 K temperature variations. For particle size analyses, Malvern NANO-S90 Zetasizer employing He−Ne laser (633 nm) was used at a scattering angle of 90° at room temperature. The chemical composition of synthesized NPs was confirmed by EDX using Phillips XL 30 EDX unit. TEM studies of palladium NPs were performed by redispersing the samples in ethanol using Hitachi (H 7500) instrument, operated at an accelerating voltage of 100 kV. Freshly prepared samples were gently placed over 200-mesh copper grid uniformly coated with carbon film. XRD spectrum was recorded on Panalytical X'Pert Pro X-ray diffractrometer equipped with Cu Kα radiation (1.5406 Å) operating at 40 kV, with scanning speed of 8°/min to examine the crystalline phase of the sample by forming a film on a glass slide. To prepare glass slide Pd NPs were redispersed in hexane. The particle size analysis of Pd NP was performed in DCM. Fluorescence studies were performed using Hitachi F-7000 instrument containing xenon lamp, where sample was excited at 270 nm with scan speed of 500 nm. The slit width was kept at 10 nm. Palladium NPs were suspended in mixture of absolute alcohol and distilled water in the ratio of 2:8 for fluorescence studies. SAXS was performed using Anton Paar SAXSpace. For the measurements, ID3003-Cu Kα X-ray generator (α = 0.1542 nm) was used. The instrument was operated at 40 kV, 50 mA with beam collimation line = 0.3 × 20 mm. The sample temperature in quartz cuvette was controlled with a thermostated sample holder unit at 24 °C. The scattered intensities were measured with Mythen detectors (exposure time, 30 min). SAXS data were processed (background−subtraction $p(r)$ calculation) with the programs SAXStreat and SAXSquant. Data evaluation was performed with programs GIFT (Fourier transform) and DECONS (electron density). The sample of **complex 1** was prepared in DCM at 5 times higher concentration of its critical micellar concentration (cmc).

Synthesis of Complex 1. **Complex 1** was synthesized using ligand insertion method[39] by reacting $PdCl_2$ with dodecylamine in 1:2 stoichiometry. Palladium(II) chloride (0.4 mmol, 0.095 g) and dodecylamine ($C_{12}H_{25}NH_2$) (0.8 mmol, 0.148 g) were dissolved in 20 mL of dry DMF in a round-bottomed flask (Scheme 1). Reaction mixture was heated at 338 K for 2 h with vigorous stirring. On the

DOI: 10.1021/acs.inorgchem.5b01171
Inorg. Chem. 2015, 54, 9002−9012

Scheme 1. Synthesis of Bisdodecylaminepalladium(II) Chloride Complex

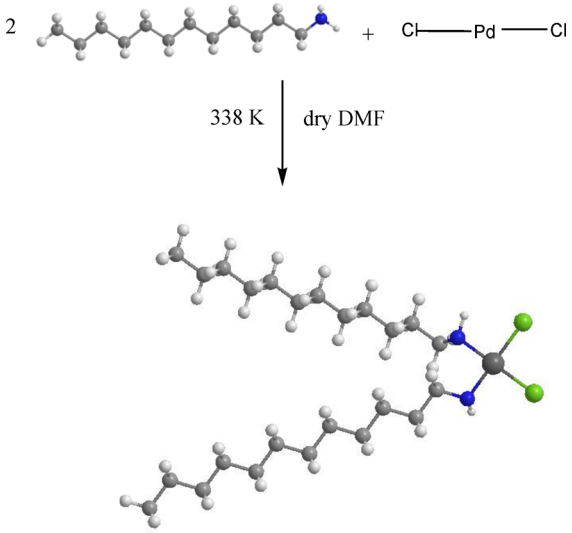

completion of reaction, change in color from dark red to light yellow was observed, and yellowish crystalline product was isolated. Further, recrystallization was done with absolute alcohol, and product obtained was stored in desiccator. **Complex 1** was readily soluble in organic solvents and sparingly soluble in water. Yield: 181.94 mg (0.332 mmol, 83%). mp 396 K. Anal. Calcd (%) for $(C_{12}H_{25}NH_2)_2PdCl_2$: C, 52.54; H, 9.84; N, 5.16; found C, 52.68; H, 9.82; N, 4.97. IR: (KBr) $\tilde{\nu}$/cm^{-1} 2955 (m), 2848 (m), 3214 (s), 1537 (m), 1413 (m), 1367 (m), 470 (sh). NMR: δ, ppm 2.65 (s, 4H), 1.58 (s, 8H), 1.19 (s, 38H), 0.81 (s, 4H). Time-of-flight mass spectrometry (TOF-MS): electrospray (ES^+; MeOH), m/z calcd for $[Pd(C_{12}H_{25}NH)_2Cl_2]^+$: 547.71; found: 547.72. m/z for $(C_{12}H_{25}NH)^+$ 185.36. m/z for $[PdC_{12}H_{25}NH_2Cl_2]^+$: 362.3. m/z for $[PdC_{12}H_{25}NH_2Cl]^+$: 327.4.

Preparation of Metallomicelles and Their Characterization. Metallomicelles were prepared in different alcohols. The measurement of conductivity was performed with 5 mL of sample followed by dilution for a temperature range of 20−40 °C with accuracy up to ±3%. To estimate the hydrodynamic radius of micelles, samples were prepared at a concentration 5 times the critical micellization concentration (cmc) in ethanol, propanol, and butanol. The samples were filtered with 0.2 μm filter.

Synthesis and Characterization of Palladium Nanoparticles. The NPs of palladium were synthesized by a two-phase (water/DCM) redox reaction.[40] Freshly prepared aqueous solution of $NaBH_4$ (10 mM, 10 mL) was added dropwise to **complex 1** (2 mM, 10 mL) dissolved in DCM, and the reaction mixture was stirred vigorously for 2 h. Higher molar ratio of $NaBH_4$ was used to ensure the complete reduction of metal ions to zerovalent metallic state. Yellow color of the reaction mixture turned black and remained suspended in DCM. The organic phase in equilibrium with colorless aqueous phase was separated and dried under vacuum rota-evaporator to obtain powdered black NPs of metallic palladium. The NPs were further dried in vacuum desiccator for 2 d prior to characterization.

Cytotoxicity Studies. **Complex 1** was screened for cytotoxicity in concentration range from 5 to 25 μg/mL in DCM. Vero cell lines at a density of 1×10^4 per well were cultured in a 100 μL volume of cell culture medium in a 96-well cell culture plate in MEM media containing 5% FBS. The experiments were performed in triplicates. Cells were allowed to incubate for proliferation at 37 °C in 5% CO_2 incubator for 24 h. The cells were further incubated with varying concentrations of **complex 1** for 24 h. Untreated cells were taken as reference. Medium without cells was also taken in three wells for correction of background coloration. After incubation, the cultures were removed from incubator into laminar flow hood, and 10 μL of Resazurin solution prepared in EMEM media (1 mg/mL at 4 °C for 20 min) was added in all wells and incubated for 24 h. After 4 h, the pink colored Resorufin is formed, and absorbance was observed by spectrophotometer (ELISA plate reader) at wavelength 573 nm. Cytotoxicity percentage was calculated with reference to untreated cells after normalizing the background coloration of media.

$$\%\text{cytotoxicity} = \frac{\text{abs}_u - \text{abs}_t}{\text{abs}_u} \times 100 \quad (1)$$

where abs_u is the absorbance of cells not treated with **complex 1**, and abs_t is the absorbance of cells treated with **complex 1**.

Antimicrobial Studies. In vitro antimicrobial tests were performed using growth inhibitory zone well method[41,42] against three pathogenic microorganisms, that is, Gram-positive (*Bacillus cereus* ITCC 240) and Gram-negative (*Klebsiella pneumoniae* ITCC 138) bacteria and a fungi (*Curvularia lunata* ITCC 6257). Bacteria were cultured on nutrient agar broth, and fungi was cultured on potato dextrose agar broth media incubated at 37 °C for 24 h. Broths were autoclaved for 2 h before spreading the microbial stains. Antimicrobial activities of test samples were compared with standard drug *Ceftriaxone* (5 μg/mL). Test samples (60 μL; 5 μg/mL prepared in DCM) were added to 6 mm well bored on agar plates after homogeneous pouring of freshly cultured microbial stains. After overnight incubation at 37 °C, diameters of inhibition zones were measured to nearest millimeter, and average value of triplicate measurement is reported. Diameter of the well was excluded from inhibition zone diameter. DCM was used as negative control, and it did not show any inhibitory activity. Minimum inhibitory concentration (MIC) studies were performed by multiple dilutions until further zone of inhibition was minimized to nil.

RESULTS AND DISCUSSION

Synthesis and Characterization of Metallosurfactant. A neat one-pot synthesis of solvophobic bisdodecylamine-palladium(II) chloride (**complex 1**) was performed without formation of any side products. Elemental composition of **complex 1** was estimated using CHN, and relative percentages of C, H, and N obtained were in excellent agreement with the calculated values. Various other spectroscopic techniques were employed to get insight of structure of the **complex 1** in both solid and solution. To verify the mode of complexation of ligand (dodecylamine) with palladium ions, FTIR and NMR spectra of pure ligand and **complex 1** were compared (Figure S1a−c). FTIR results showed a strong band at 470 cm^{-1} corresponding to ν-sym stretching of metal nitrogen (Pd−N) coordinate bond. The bands observed at 3336 cm^{-1} (ν-sym N−H stretching) and 1577 cm^{-1} (in-plane bending δ-sym N−H group) for pure dodecylamine showed decrease in stretching frequency to 3214 and 1537 cm^{-1}, respectively (Table S1, Supporting Information), because of transfer of electron density from ligand to metal via metal−ligand coordination. Similar results were also obtained by ^{1}H NMR spectroscopy (Figure S1b,c). Signal obtained at δ = 2.65 ppm was assigned to the NH_2 protons, and signal at δ = 1.58 ppm was assigned to methylene protons of CH_2NH_2 group. A broad signal obtained at δ = 1.19 ppm was assigned to methylene groups of two hydrocarbon chains, and signal obtained at δ = 0.81 ppm was assigned to terminal methyl groups of two hydrocarbon chains. In comparison to dodecylamine, **complex 1** gave ^{1}H resonances with downfield shifts due to transference of electron density from -NH_2 of the ligand to palladium ions, approving the complexation. The presence of molecular entity/fragments as depicted by mass spectrometry is shown in Figure S1d, and Figure S2 gives plausible decomposition mechanism deciphered from mass spectrum.

X-ray Crystallography Studies. For further structural details, X-ray crystallography studies of **complex 1** were done.

DOI: 10.1021/acs.inorgchem.5b01171
Inorg. Chem. 2015, 54, 9002−9012

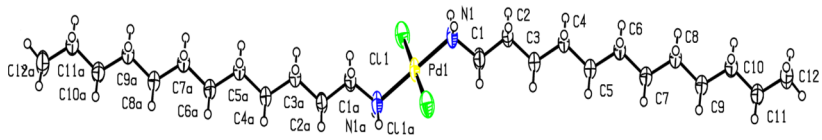

Figure 1. Perspective view of **complex 1**.

Colorless, needlelike single crystals of **complex 1** were grown in methanol by slow evaporation at room temperature. The structure was solved and refined using the Bruker SHELXTL Software Package, using the space group P 1 21/c 1, with $Z = 2$ for the formula unit, $C_{24}H_{54}Cl_2N_2Pd$ having a monoclinic crystal. Pd(II) was coordinated by dodecylamine ligands oriented in trans geometry (Figure 1) with N−Pd−N bond angle of 179.997° and mean Pd−N bond length of 2.035 Å. Density of the crystal was found to be 1.292 mg/cm^3. A summary of crystallographic data, bond lengths, and bond angles for **complex 1** are given in Tables 1−3 and Table S2 of the Supporting Information.

To check the thermal stability of **complex 1**, TGA analysis using nonisothermal conditions was performed. Mainly two major mass loss regions were observed (Figure 2): the first mass loss region is from 200 to 290 °C, and the second mass loss region is from 300 to 600 °C. In the first step, both complexed dodecylamine moieties decomposed simultaneously and leave metal chloride as residue, which further decomposed to metal in the second step (Scheme 2). According to the proposed decomposition patterns, theoretical mass loss

Table 1. Sample and Crystal Data of Complex 1 with Structure Refinement

chemical formula	$C_{24}H_{54}Cl_2N_2Pd$	
formula weight	547.99	
temperature	296(2) K	
wavelength	0.710 73 Å	
crystal size	0.30 × 0.30 × 0.50 mm	
crystal habit	colorless rod shaped	
crystal system	monoclinic	
space group	P 1 21/c 1	
unit cell dimensions	a = 5.8218(4) Å	α = 90°
	b = 7.0123(5) Å	β = 92.428(3)°
	c = 34.528(2) Å	γ = 90°
volume	1408.31(17) Å^3	
Z	2	
density (calculated)	1.292 mg/cm^3	
absorption coefficient	0.861 mm^{-1}	
F(000)	584	
θ range for data collection	1.18° to 25.10°	
index ranges	$-3 \le h \le 6$, $-8 \le k \le 7$, $-40 \le l \le 41$	
reflections collected	8991	
independent reflections	2495 [R(int) = 0.0357]	
coverage of independent reflections	99.7%	
absorption correction	multiscan	
structure solution technique	direct methods	
structure solution program	SHELXS-97 (Sheldrick, 2008)	
refinement method	full-matrix least-squares on F^2	
refinement program	SHELXL-97 (Sheldrick, 2008)	
function minimized	$\sum w(F_o^2 - F_c^2)^2$	
data/restraints/parameters	2495/0/134	
goodness-of-fit on F^2	0.991	
final R indices	2024 data; $I > 2\sigma(I)$ all data	$R1$ = 0.0264, $wR2$ = 0.0835
		$R1$ = 0.0381, $wR2$ = 0.1038
weighting scheme	$w = 1/[\sigma^2(F_o^2) + (0.0677P)^2 + 0.3593P]$ where $P = (F_o^2 + 2F_c^2)/3$	
largest diff peak and hole	0.316 and −0.451 e Å^{-3}	
R.M.S. deviation from mean	0.113 eÅ^{-3}	

Table 2. Important Bond Lengths (Å) of Complex 1

Pd1−N1	2.035(2)	Pd1−N1#1	2.035(2)
Pd1−Cl1#1	2.2974(9)	Pd1−Cl1	2.2975(9)
N1−C1	1.481(4)	N1−H1A	0.9
N1−H1B	0.9	C1−C2	1.509(4)
C1−H1C	0.97	C1−H1D	0.97
C2−C3	1.515(4)	C2−H2A	0.97
C2−H2B	0.97	C3−C4	1.518(4)
C3−H3A	0.97	C3−H3B	0.97
C4−C5	1.513(4)	C4−H4A	0.97
C4−H4B	0.97	C5−C6	1.517(4)
C5−H5A	0.97	C5−H5B	0.97
C6−C7	1.515(4)	C6−H6A	0.97
C6−H6B	0.97	C7−C8	1.521(4)
C7−H7A	0.97	C7−H7B	0.97
C8−C9	1.511(4)	C8−H8A	0.97
C8−H8B	0.97	C10−C11	1.512(4)
C10−C9	1.520(4)	C10−H10A	0.97
C10−H10B	0.97	C11−C12	1.515(4)
C11−H11A	0.97	C11−H11B	0.97
C12−H12A	0.96	C12−H12B	0.96

Table 3. Important Bond Angles (deg) of Complex 1

N1−Pd1−N1#1	179.9970(10)	N1−Pd1−Cl1#1	91.45(8)
N1#1−Pd1−Cl1#1	88.55(8)	N1−Pd1−Cl1	88.55(8)
N1#1−Pd1−Cl1	91.45(8)	Cl1#1−Pd1−Cl1	180.0
C1−N1−Pd1	113.47(19)	C1−N1−H1A	108.9
Pd1−N1−H1A	108.9	C1−N1−H1B	108.9
Pd1−N1−H1B	108.9	H1A−N1−H1B	107.7
N1−C1−C2	114.5(3)	N1−C1−H1C	108.6
C2−C1−H1C	108.6	N1−C1−H1D	108.6
C2−C1−H1D	108.6	H1C−C1−H1D	107.6
C1−C2−C3	111.8(2)	C1−C2−H2A	109.3
C3−C2−H2A	109.3	C1−C2−H2B	109.3
C3−C2−H2B	109.3	H2A−C2−H2B	107.9
C2−C3−C4	114.6(2)	C2−C3−H3A	108.6
C4−C3−H3A	108.6	C2−C3−H3B	108.6
C4−C3−H3B	108.6	H3A−C3−H3B	107.6
C5−C4−C3	113.7(2)	C5−C4−H4A	108.8
C3−C4−H4A	108.8	C5−C4−H4B	108.8
C3−C4−H4B	108.8	H4A−C4−H4B	107.7
C4−C5−C6	114.3(2)	C4−C5−H5A	108.7
C6−C5−H5A	108.7	C4−C5−H5B	108.7
C6−C5−H5B	108.7	H5A−C5−H5B	107.6
C7−C6−C5	113.8(2)	C7−C6−H6A	108.8
C5−C6−H6A	108.8	C7−C6−H6B	108.8
C5−C6−H6B	108.8	H6A−C6−H6B	107.7

DOI: 10.1021/acs.inorgchem.5b01171
Inorg. Chem. 2015, 54, 9002−9012

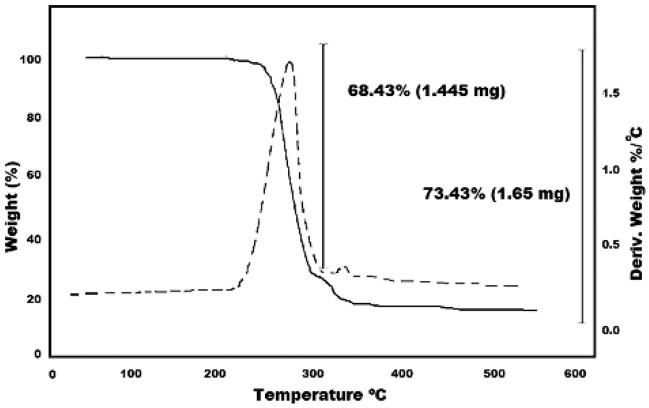

Figure 2. TGA (solid line) and differential thermal analysis (dotted line) curves of **complex 1**.

Scheme 2. Plausible Thermogravimetric Decomposition Pattern of Complex 1

$$[M(CH_3(CH_2)_{11}NH_2)_2Cl_2]_{(S)} \rightarrow MCl_{2(S)} + 2CH_3(CH_2)_{11}NH_{2(g)} \quad (2)$$

$$MCl_{2(S)} \rightarrow M_{(s)} + Cl_{2(g)} \quad (3)$$

percentages were calculated and were found in excellent agreement with experimental values obtained from TGA graph as summarized in Table 4.

Table 4. Thermogravimetric Analysis of Complex 1

transition temperature (°C)	calculated mass loss (%)	observed mass loss (%)
268.7	68.25	68.43
328.6	73.25	73.43
values of activation energy calculated for the first decomposition step of **complex 1**		
methods	E, kJ mol^{-1}	R
Horowitz–Metzger	23.15	0.991
Coats–Redfern	22.43	0.996
Madhusudanan–Krishnan–Ninan	27.20	0.985
Wanjun–Yuwen–Hen–Cunxin	23.61	0.993
Van Krevelen	26.55	0.988

Five different nonisothermal methods,[43] namely, those of Horowitz–Metzger, Coats–Redfern, Madhusudanan–Krishnan–Ninan, Wanjun–Yuwen–Hen–Cunxin, and Van Krevelen, were employed to determine the activation energy for the first decomposition step of **complex 1** (Table 4) by plotting linearization curves. The details of equations are as follows:

For solid-state reaction, rate constant (k) is calculated by kinetics equation

$$\frac{d\alpha}{dt} = kf(\alpha) = A\ e^{-E/RT} f(\alpha) \quad (4)$$

where A (pre-exponential factor) and E (activation energy) are the Arrhenius parameters; α is the fractional reaction; t is time; R is the gas constant; T is temperature in Kelvin, and $f(\alpha)$ is the kinetics function.

In isothermal kinetics studies, the rate constant is given by

$$g(\alpha) = kt \quad (5)$$

where, $g(\alpha) = \int_0^\infty ((d\alpha)/f(\alpha))$ can be calculated by the integration of $f(\alpha)$.

Under non-isothermal conditions, in which a sample is heated at a constant rate $\beta = dT/dt$, the explicit temporal in eq 4 is eliminated through the trivial transformation, so that $T = T_0 + \beta$, where T_0 is the starting temperature and T is the temperature at any time t. Upon integration, eq 4 may be written as

$$g(\alpha) = \frac{A}{\beta}\int_{T_0}^{T} e^{-E/RT}\, dt \quad (6)$$

Doyle's equation leads by integration of eq 6 by considering that reaction rate is negligible at low temperatures.

$$g(\alpha) = \frac{AE}{R\beta}\int_{T_0}^{T}\frac{e^{-x}}{x} - \int_0^\infty \frac{e^{-u}}{u}du = \frac{AE}{R\beta}P(x) \quad (7)$$

where $u = E/RT$, and x is the corresponding value of u at which a fraction of material was decomposed. The above equation can be reformulated as

$$\ln g(\alpha) - \ln P(x) = \frac{AE}{R\beta} = B \quad (8)$$

where B is a constant for a particular reaction at a constant heating rate. The integral function $P(x)$ has no analytical solution; it may be written in an expanded form and estimated by using a procedure of trial-and-error type involving iteration.

(i) Coats–Redfern method

$$g(\alpha) = \frac{ART^2}{\beta E}\left[1 - \frac{2RT}{E}\right]e^{-E/RT} \quad (9)$$

So the equation takes the form

$$-\ln\frac{g(\alpha)}{T^2} = -\ln\frac{AR}{\beta E}\left[1 - \frac{2RT}{E}\right] + \frac{E}{RT} \quad (10)$$

The fraction mass loss (α) and corresponding $(1-\alpha)^n$ are calculated from TG curves, where n depends upon the reaction model.

$$-\log\frac{1-(1-\alpha)^{1-n}}{T^2(1-n)} = \log\frac{AR}{\beta E}\left[1 - \frac{2RT}{E}\right] - \frac{E}{2.303RT} \text{ for } n \neq 1 \quad (11)$$

$$-\log\frac{-\log(1-\alpha)}{T^2} = \log\frac{AR}{\beta E}\left[1 - \frac{2RT}{E}\right] - \frac{E}{2.303RT} \text{ for } n = 1 \quad (12)$$

In general, $2RT/E \ll 1$ exhibits a small variation with T. So, it is assumed that the term $(1 - 2RT/E)$ is approximately constant and equal to unity. Therefore, plotting the left-hand side of the above equations against $1/T$ gives the slope $-2.303E/R$, which yields the value of activation energy, and the intercept gives value of A with excellent correlation coefficients, which indicates a good fit of the linear function.

(i) Madhusudanan method

$$-\ln\frac{g(\alpha)}{T^{1.9206}} = -\ln\frac{AR}{\beta E} + 3.7678 - 1.9206\ln E - 0.12040\frac{E}{RT} \quad (13)$$

(ii) Wanjun–Yuwen–Hen–Cunxin method

DOI: 10.1021/acs.inorgchem.5b01171
Inorg. Chem. 2015, 54, 9002–9012

Scheme 3. Depicting the Bilayer Formation by the Double-Chained Metallosurfactant

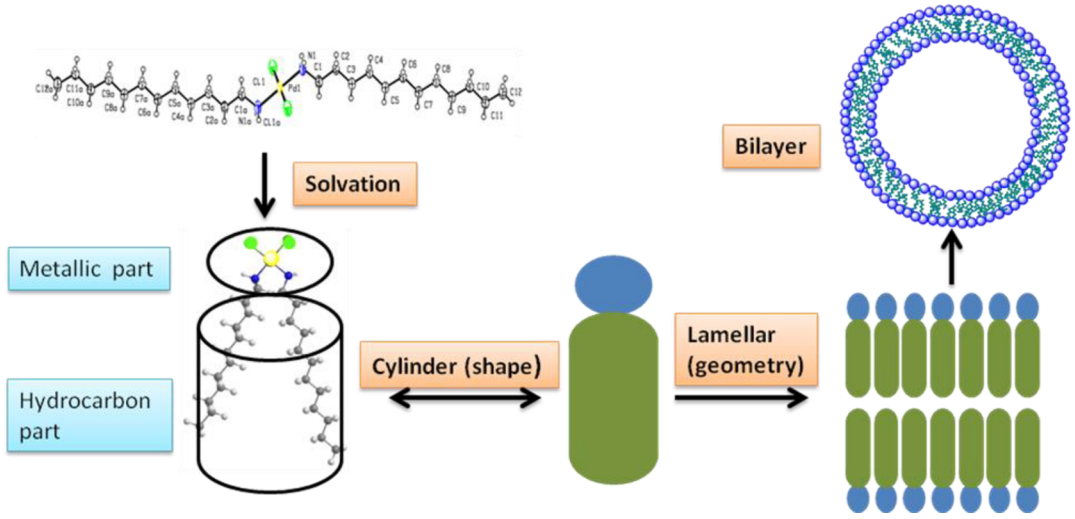

$$-\ln \frac{g(\alpha)}{T^{1.8946}} = -\ln \frac{AR}{\beta E} + 3.6350 - 1.8946 \ln E - 1.0014\frac{E}{RT} \quad (14)$$

(iii) Van Krevelen method

$$\ln g(\alpha) = \ln\left(\frac{A(0.368/T_m)^{E_a/RT_m}}{\beta\left(\frac{E_a}{RT_m}+1\right)}\right) + \left(\frac{E_a}{RT_m}+1\right) \ln T \quad (15)$$

(iv) Horowitz–Metzger method, a new parameter $T = T_m + \theta$ was introduced. If the order of reaction is 1, T_m is defined as the temperature at which $(1-\alpha)_m = 1/e = 0.368$, and the final expression is

$$\ln \ln(\alpha) = \frac{E\theta}{RT_m^2} \quad (16)$$

In the above equations; α, $g(\alpha)$, β, T_m, E, A, R are the degree of reaction, integral function of conversion, heating rate, differential thermogravimetric peak temperature, activation energy (kJ mol^{-1}), pre-exponential factor (min^{-1}), and gas constant (8.314 J mol^{-1} K^{-1}), respectively. All the above-mentioned methods are based on a single heating rate in the thermal analysis. The values of activation energy obtained from all the above-mentioned methods were comparable, and the mean value of 24.58 kJ mol^{-1} was obtained.

Self-Aggregation Behavior. After the preparation and characterization of **complex 1**, it was utilized for the fabrication of NPs. Since **complex 1** is a double chain structure with long hydrocarbon chains, the micellar templates were explored for the preparation of NPs. Micelles as templates were chosen for simplicity; however, because **complex 1** have limited aqueous solubility and to understand the formation of metallomicelles of **complex 1**, alcohols were selected as medium.[44] A similar attempt with solvophobic palladium dodecylammonium acetate complex had been made earlier,[43] where metallomicelles were studied in *n*-alcohols. Keeping this in view, the micellization behavior of **complex 1** in ethanol, propanol, and butanol was investigated. The trans form[45,46] of **complex 1** aggregates in alcohols to yield a bilayer structure; because of double chain, it attains a cylindrical shape that packs itself in lamellar geometry and finally leads to the formation of bilayer as shown in Scheme 3. The critical micellization concentrations (cmc) were estimated with variation in temperature and dielectric constant of the medium (Figure 3). The cmc decreased with increase in

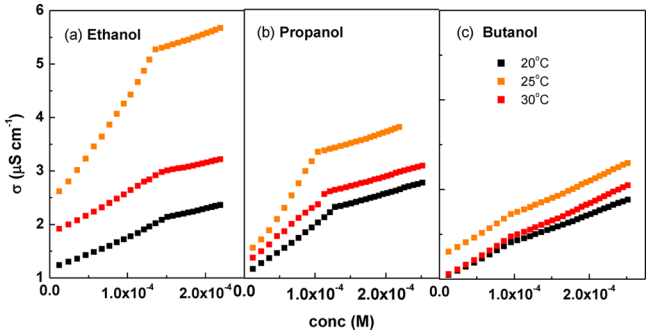

Figure 3. Temperature dependence of specific conductivity vs concentration of complex 1 in different *n*-alcohols.

temperature and decrease in dielectric constant from ethanol to butanol (Table S3). Temperature variation results in two competitive effects. First, the temperature increase causes a decrease in solvation of the hydrophilic group, which favors micellization. Second, the temperature increase also causes a disruption of the solvent cage surrounding the hydrophobic group, and this retards micellization. The lowering of cmc with increase in temperature is probably due to the decrease in solvation of the hydrophilic group. However, the decrease in cmc with change in dielectric constant is due to less favorable interactions between the polar groups of the surfactant and alcohols causing micellization to occur at relatively lower concentrations.[44]

The thermodynamic parameters of micellization were also estimated, and the standard Gibbs free energy of micelle formation per mole of monomer is given by

$$\Delta G_m^o = (2-\beta)RT \ln X_{cmc} \quad (17)$$

where R, T, β, and X_{cmc} represents gas constant, absolute temperature, degree of ionization, and cmc in terms of mole

DOI: 10.1021/acs.inorgchem.5b01171
Inorg. Chem. 2015, 54, 9002–9012

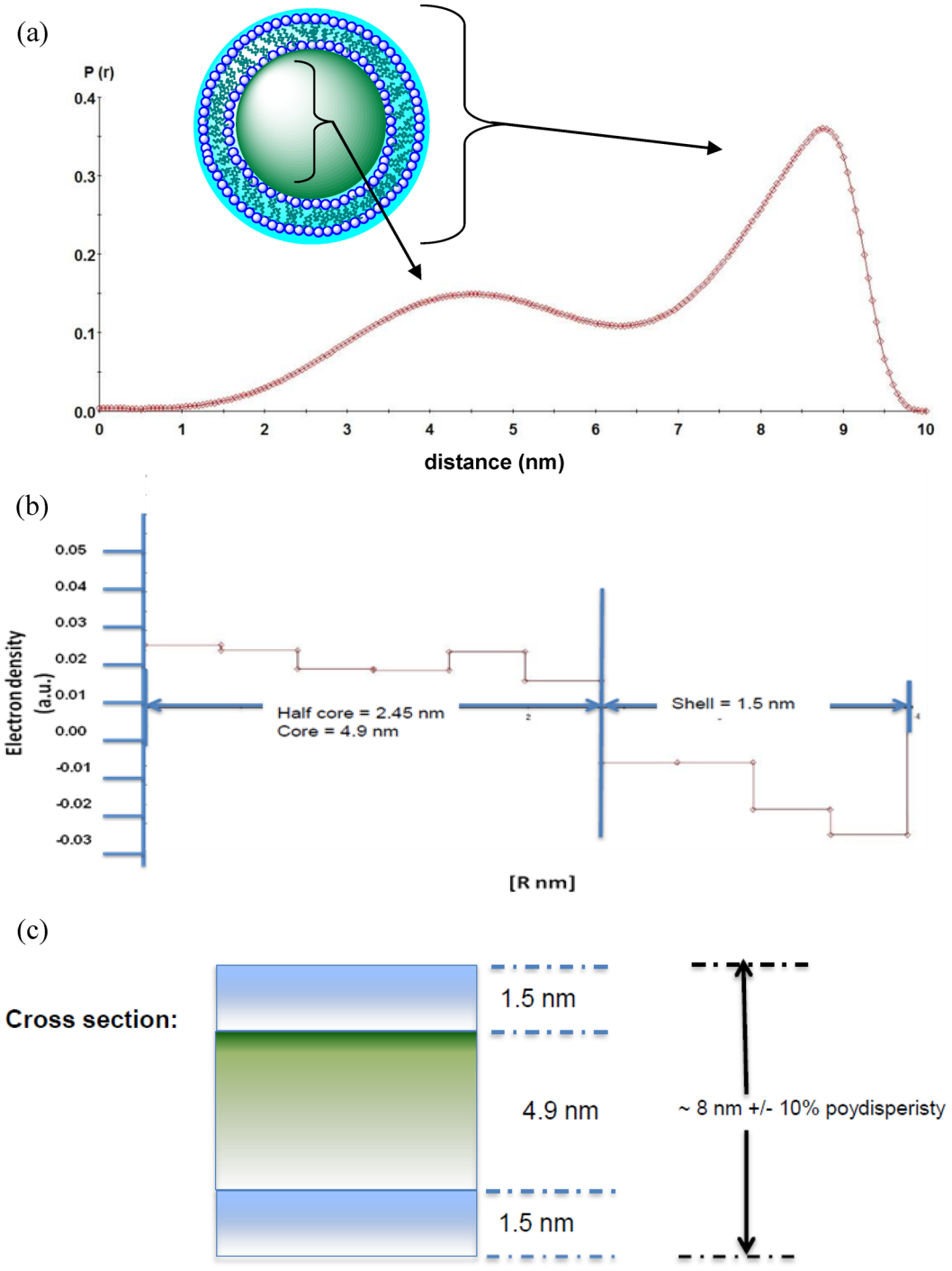

Figure 4. (a) Pair-distance distribution functions $p(r)$ and (b,c) electron density as a function of distance for **complex 1** in DCM.

fraction, respectively. The values obtained for Gibbs free energy (Table S3) were found to be more negative showing that the overall micellization process is spontaneous and thermodynamically favored. The estimation of enthalpy of micellization is estimated through Gibbs−Helmholtz relation.

$$\Delta H_m^o = -RT^2(2-\beta)\frac{d \ln X_{cmc}}{dt} \quad (18)$$

The entropy of micellization is estimated by the following equation.

$$\Delta S_m^o = (\Delta H_m^o - \Delta G_m^o)/T \quad (19)$$

The enthalpy and entropy of micellization in the present case were found to be positive. ΔG_m^o is the sum of the enthalpic (ΔH_m^o) and entropic (ΔS_m^o) contributions. In case of ethanol, enthalpy factor contributes 25% toward free energy of micellization, and process is entropy driven. However, for propanol and butanol, the process is enthalpy driven. The micelles and/or reverse micelles are dynamic entities and polydisperse in nature. The hydrodynamic sizes of metallomicelles as estimated using DLS were 150 nm in ethanol, 160 nm in propanol, and 168 nm in butanol. The size was found to increase with increase in the hydrophobicity of alcohols.[43] The

DOI: 10.1021/acs.inorgchem.5b01171
Inorg. Chem. 2015, 54, 9002−9012

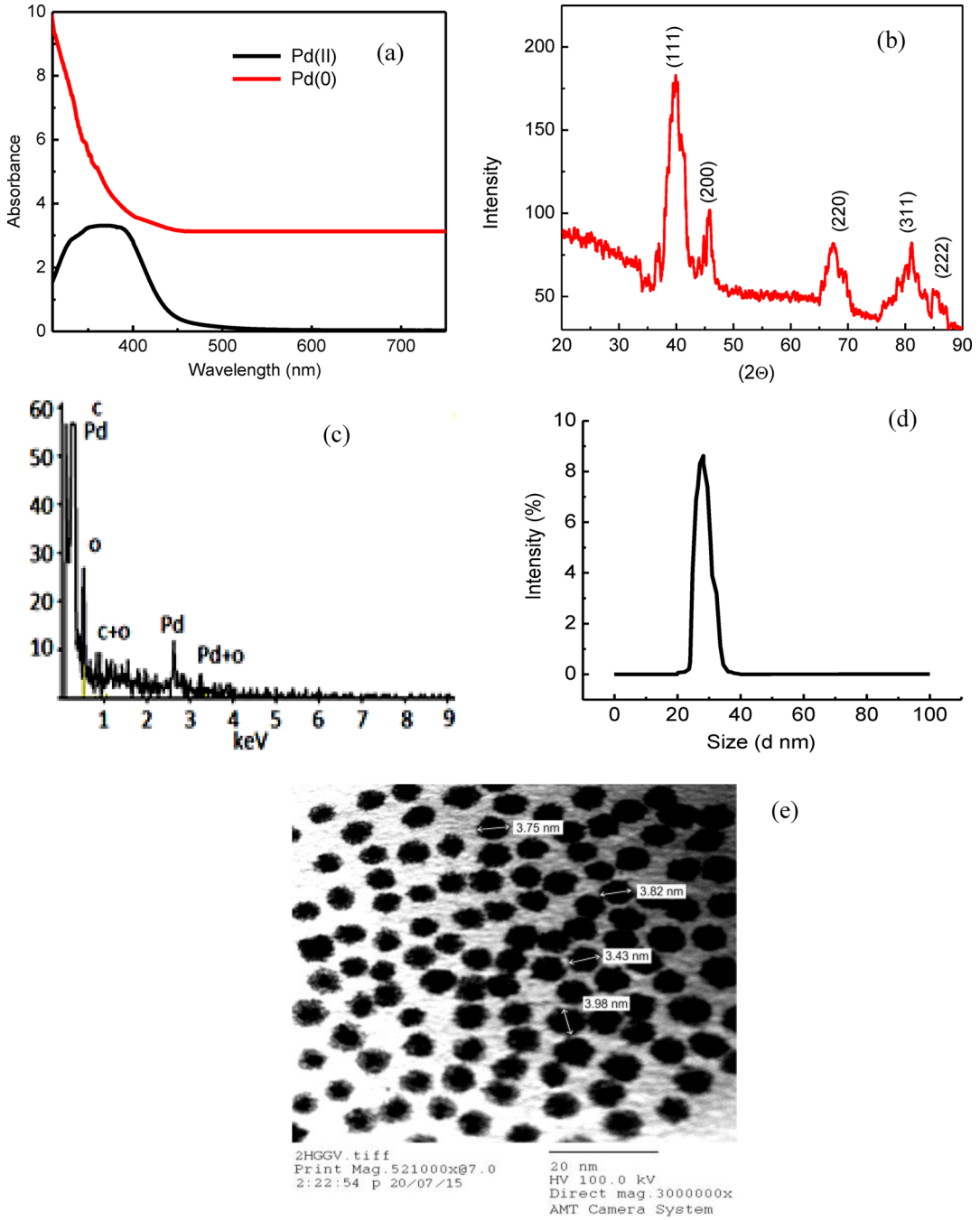

Figure 5. (a) UV−visible spectra of Pd NPs (red) and $PdCl_2$ (black). (b) XRD pattern, (c) EDX and (d) DLS spectra, and (e) TEM image of Pd NPs.

particle size analyses data are given in Supporting Information as Figure S3.

Synthesis of Palladium Nanoparticles. In past decade nanotechnology has engulfed all areas of research; still, the thrust for finding a simple and viable method for its preparation is never-ending. Redox method was employed to prepare Pd NPs, and synthesis was performed using two-phase (water/DCM) system, where in one phase micelles exit. This route offers many advantages such as use of a simple reducing agent, avoiding harsh conditions, and tedious purification procedures. The route of synthesis of NPs via micellar template offers a microenvironment for the generation of NPs by means of arrested growth mechanism.[47]

For executing this method, two immiscible (or partially miscible) layers are required, and that is a reason DCM/water system was selected (instead of alcohols). However, it was not possible to measure aggregation behavior of **complex 1** in DCM via conductivity method. Therefore, the confirmation of the formation of aggregates in DCM was made using SAXS measurements. Figure 4 shows the pair-distance distribution functions (PDDF; $p(r)$; Figure 4a) and electron density (Figure 4b,c) as a function of distance. The aggregation of **complex 1** in DCM is validated from the results where PPDF gives a typical profile for inhomogeneous system, depicting a core−shell structure of the revere micelle.[48,49] The electron density

DOI: 10.1021/acs.inorgchem.5b01171
Inorg. Chem. 2015, 54, 9002−9012

measurements reveal that core diameter (of revere micelle) is of the range 4−5 nm and the shell thickness of 1.5−2 nm.

As-fabricated Pd NPs in micellar core were characterized by UV−visible, XRD, EDX, TEM, and DLS. For UV−visible studies, samples were suspended in absolute alcohol. UV−visible spectrum of $PdCl_2$ along with reduced sample is shown in Figure 5a. Palladium(II) chloride (black line) showed a broad absorption at wavelength 360 nm. However, metallic palladium (red line) showed exponential decrease in absorption intensity, and no peak ca. 300 to 400 nm was observed, which indicated complete reduction[50] of palladium(II) to palladium (0). The oxidation state of Pd was further confirmed using XRD. The XRD pattern (Figure 5b) gave peaks for (111), (200), (220), (311), and (222) planes and are in good agreement with JCPDS standard (No. 05−0681) for metallic Pd.[51,52] The chemical composition was confirmed by EDX (Figure 5c). Higher carbon content (93.00%) as compared to palladium (5.32%) revealed that the NPs were stabilized by hydrocarbon chains of surfactant (Table S4). The shape, size, and morphology were determined by DLS (Figure 5d) and TEM (Figure 5e). TEM micrograph revealed formation of highly monodispersed and spherical NPs with average size of 3−5 nm. These Pd(0) are in contact with the hydrocarbon chains from a very early stage of the reaction; therefore, they did not allow the agglomeration, and in turn these metallomicelles controlled the aggregation effectively. However, hydrodynamic size of NPs obtained from DLS was found to be 28 nm because DLS takes into account the ligand shell with trapped solvent, whereas TEM visualizes only inorganic metallic core.[53] This method of NP preparation has proved to be efficient in terms of size control, good yield, and easy extraction. A surfactant layer is expected to form on the surface of NPs, which prevents aggregation and ensures the long-term stability of the NPs. Moreover, precursor **complex 1** can function as both the metal ion provider and the capping agent.

Further, interactions of fabricated palladium NPs were monitored with BSA.[54] Figure S4 shows the effect of concentration of NPs on the intrinsic fluorescence intensity of BSA. It could be inferred that, with gradual increase in the concentration of Pd NPs (0.5−3.5 μg per 10 mL) in aqueous solution of BSA (10 μM), the fluorescence intensity of BSA at ∼364 nm was quenched. Presence of tryptophan (Trp) and tyrosine (Tyr) residues in the primary structure of BSA provide intrinsic fluorescence to the protein molecule. It is proposed that the addition of Pd NPs altered the microenvironment around the fluorophores and in the protein, which led to quenching of the fluorescence intensity. Slight blue shift along with quenching suggested the structural modifications in the native state of BSA, revealing interactions with palladium NPs. Binding constants were calculated using Lineweaver−Burk modified Stern−Volmer equation, that is, $(F_0 - F)^{-1} = F_0^{-1} + K_a^{-1} F_0^{-1} [Q]^{-1}$, where F_0 is the fluorescence intensity in the absence of quencher, F is the fluorescence intensity in the presence of quencher, $[Q]$ is the concentration of quencher, and knowing the slope of the above equation, the binding constant K_a was found to be 79 876.43 L mol^{-1} (R = 0.9951).

Antimicrobial Assay of Metallosurfactant and Pd Nanoparticles. To investigate the biological potential of prepared **complex 1** and its NPs, the in vitro antimicrobial activity against three pathogenic microorganisms, namely, *Bacillus cereus*, *Klebsiella pneumoniae*, and *Curvularia lunata* was studied using growth inhibitory zone plate well method. Table 5 shows the comparison of antimicrobial activity of metallosurfactant and the corresponding metallic NPs. Antimicrobial activity of metallosurfactant was higher than parent surfactant. This is attributed to the fact that incorporation of metal ion increases the adsorption tendency of parent surfactant. Pd NPs showed best results against fungal strain (comparable to the standard drug). The high activity of NPs could be attributed to remarkably high surface area of ligand-protected metallic NPs so that these might show extensive adsorption or permeation through the cell wall leading to alterations in the functioning of cytoplasmic organelles, ultimately resulting in death of the cell.

Table 5. Comparison of Antimicrobial Activity of Complex 1 and Pd NPs

methods	sample	microorganisms		
		Bacillus cereus	*Klebsiella pneumoniae*	curvularia lunata
average IZ[a] (mm)	dodceylamine	12	11	12
	complex 1	24	16	18
	Pd NPs	38	18	48
	Ceftriaxone	66	58	52
MIC[b] (μg/mL)	**complex 1**	3.0	4.0	3.0
	Pd NPs	0.6	0.8	0.5

[a]Inhibition zone diameter. [b]Minimum inhibitory concentration.

Cytotoxicity of Complex 1. To accomplish biocompatibility of prepared **complex 1**, for the further utilization of prepared micellar assembly and NPs as vectors (for drugs and dyes), it was essential to study the cytotoxic response on healthy cells. As shown in Figure 6, different concentrations of

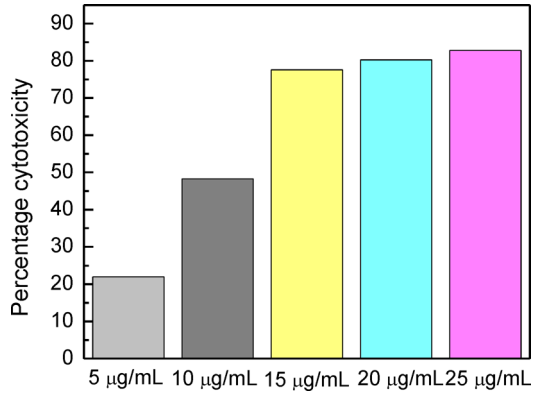

Figure 6. Percentage cytotoxicity of **complex 1** as a function of concentration.

complex 1 (ranging from 5 to 25 μg/mL) were incubated in a 96 well plate containing Vero cell lines[55] at a density of 1×10^4 for 24 h. Thereafter, 20 μL of Reasazurin dye was poured in the wells, and these mixtures were incubated for 4 h. Finally absorbance at 590 nm was observed with spectroflorometer, and cytotoxicity was measured. Toxicity response of healthy cells was concentration-dependent, and IC_{50} value was found to be 10 μg/mL. For the purpose of clarity, the error bars for the standard deviation on the data were deleted; however, in all cases, the error was <10.0%.

Summary. A novel palladium-based double-chained complex was successfully synthesized using ligand insertion method. Single crystals of Pd(II) complex confirmed trans coordination of dodecylamine ligands, and TGA was used to estimate its

DOI: 10.1021/acs.inorgchem.5b01171
Inorg. Chem. 2015, 54, 9002−9012

thermal stability and kinetics of decomposition. The **complex 1** formed metallomicelles in alcohols, and the process is thermodynamically spontaneous in nature. Micellization has been confirmed using SAXS measurements, where core−shell spherical micelles were formed with 4−5 nm core size. Using same precursor and two-phase redox method, highly monodispersed metallic NPs with spherical morphology were fabricated. Average size of Pd NPs was found to be 3−5 nm because of the same size of core of micelles in which they were being formed. The NPs were further characterized using UV−visible, EDX, XRD, and DLS. With such a small size and high surface area, Pd NPs were examined for their interaction with BSA. The intrinsic fluorescence intensity of BSA at 364 nm was quenched upon the gradual addition of Pd NPs. As evident from antimicrobial activity against pathogenic organisms, palladium metallosurfactant and fabricated NPs were found to be active against a broad spectrum of microorganisms. The activity of both metallosurfactant and Pd NPs was higher than that of parent surfactant, that is, dodecylamine. Cytotoxicity results revealed IC_{50} value of 10 μg/mL for healthy Vero cell lines.

■ ASSOCIATED CONTENT

Supporting Information

The Supporting Information is available free of charge on the ACS Publications website at DOI: 10.1021/acs.inorgchem.5b01171. Related crystallographic information can be obtained from the CCDC via www.ccdc.cam.ac.uk/data_request/cif(CCDC Nos. 998756).

IR, ESI-MS, and NMR spectra and TGA data of **complex 1**, EDX for Pd NPs, fluorescence spectra of Pd NPs with BSA, DLS, and thermodynamic parameters of Pd metallomicelles, atomic coordinates of **complex 1**. (PDF)

X-ray crystallographic information for **complex 1**. (CIF)

■ AUTHOR INFORMATION

Corresponding Author

*E-mail: grc22@pu.ac.in. Phone: +91-1722534406. Fax: +91-1722545074.

Notes

The authors declare no competing financial interest.

■ ACKNOWLEDGMENTS

G.R.C. would like to acknowledge SERB-DST India SB/EMEQ-166/2013 for financial support. G.K. is thankful to DST for Inspire Faculty award (IFA-12-CH-41), and P.S. is thankful to CSIR for Senior Research Fellowship. This work is supported by PURSE II grant. Authors also want to acknowledge Dr. Mandal (Indian Institute for Science Education and Research, Mohali) for providing single-crystal X-ray data and Dr. B. N. Tripathi, (Director, National Research Centre on Equines, Hisar) for assistance in toxicity studies. Mr. P. Govasi from Anton Paar for the SAXS analysis is gratefully acknowledged.

■ REFERENCES

(1) Makarov, M. V.; Dyadchenko, V. P.; Suponitskii, K. Y.; Lemenovskii, D. A.; Antipin, M. Y. *Russ. Chem. Bull.* **2004**, *53*, 1942−1948.

(2) Saghatforoush, L. A.; Aminkhani, A.; Chalabian, F. *Transition Met. Chem.* **2009**, *34*, 899−904.

(3) Ahmadi, T. S.; Wang, Z. L.; Green, T. C.; Henglein, A.; El-Sayed, M. A. *Science* **1996**, *272*, 1924−1926.

(4) Dudev, T.; Lim, C. *Chem. Rev.* **2014**, *114*, 538−56.

(5) Nagababu, P.; Satyanarayana, S. *Polyhedron* **2007**, *26*, 1686−1692.

(6) Reetz, M. T.; De Vries, J. G. *Chem. Commun.* **2004**, *14*, 1559−1563.

(7) Kleist, W.; Pröckl, S. S.; Köhler, K. *Catal. Lett.* **2008**, *125*, 197−200.

(8) Han, W.; Liu, C.; Jin, Z. L.; Liu, N. *Chin. Chem. Lett.* **2010**, *21*, 1411−1414.

(9) Zhang, J.; Meng, X. G.; Zeng, X. C.; Yu, X.-Q. *Coord. Chem. Rev.* **2009**, *253*, 2166−2177.

(10) Morel, A.; Trzeciak, A. M.; Pernak, J. *Molecules* **2014**, *19*, 8402−8413.

(11) Lavasanifar, A.; Samuel, J.; Kwon, G. S. *J. Biomed. Mater. Res.* **2000**, *52*, 831−835.

(12) Chu, B. W. K.; Yam, V. W. W. *Inorg. Chem.* **2001**, *40*, 3324−3329.

(13) Fallis, I. A.; Griffiths, P. C.; Hibbs, D. E.; Hursthouse, M. B.; Winnington, A. L. *Chem. Commun.* **1998**, *6*, 665−666.

(14) Riyasdeen, A.; Senthilkumar, R.; Periasamy, V. S.; Preethy, P.; Srinag, S.; Zeeshan, M.; Krishnamurthy, H.; Arunachalam, S.; Akbarsha, M. A. *RSC Adv.* **2014**, *4*, 49953−49959.

(15) Pereira, R. F. P.; Valente, A. J. M.; Burrows, H. D.; de Zea Bermudez, V.; Carvalho, R. A.; Castro, R. A. E. *RSC Adv.* **2013**, *3*, 1420−1433.

(16) Srinivasan, S.; Annaraj, J.; Athappan, P. R. *J. Inorg. Biochem.* **2005**, *99*, 876−882.

(17) Amos, K. E.; Brooks, N. J.; King, N. C.; Xie, S. H.; Canales-Vazquez, J.; Danks, M. J.; Jervis, H. B.; Zhou, W. Z.; Seddon, J. M.; Bruce, D. W. *J. Mater. Chem.* **2008**, *18*, 5282−5292.

(18) Valls, E.; Solsona, A.; Suades, J.; Mathieu, R.; Comelles, F.; López-Iglesias, C. *Organometallics* **2002**, *21*, 2473−2480.

(19) Bhattacharya, S.; Snehalatha, K.; George, S. K. *J. Org. Chem.* **1998**, *63*, 27−35.

(20) Menger, F. M.; Gan, L. H.; Johnson, E.; Durst, D. H. J. *J. Am. Chem. Soc.* **1987**, *109*, 2800−2803.

(21) Van Esch, J. H.; Stols, A. L. H.; Nolte, R. J. M. *J. Chem. Soc., Chem. Commun.* **1990**, *22*, 1658−1659.

(22) Mahato, P.; Saha, S.; Choudhury, S.; Das, A. *Chem. Commun.* **2011**, *47*, 11074−11076.

(23) Dong, R.; Hao, J. *ChemPhysChem* **2012**, *13*, 3794−3797.

(24) Parera, E.; Comelles, F.; Barnadas, R.; Suades, J. *Chem. Commun.* **2011**, *47*, 4460−4462.

(25) Harraz, F. A.; El-Hout, S. E.; Killa, H. M.; Ibrahim, I. A. *J. Catal.* **2012**, *286*, 184−192.

(26) Reetz, M. T.; Westermann, E. *Angew. Chem., Int. Ed.* **2000**, *39*, 165−168.

(27) Pathak, S.; Greci, M. T.; Kwong, R. C.; Mercado, K.; Prakash, G. K. S.; Olah, G. A.; Thompson, M. E. *Chem. Mater.* **2000**, *12*, 1985−1989.

(28) Gopidas, K. R.; Whitesell, J. K.; Fox, M. A. *Nano Lett.* **2003**, *3*, 1757−1760.

(29) Deshmukh, R. R.; Rajagopal, R.; Srinivasan, K. V. *Chem. Commun.* **2001**, *17*, 1544−1545.

(30) Sangeetha, P.; Shanthi, K.; Rama Rao, K. S.; Viswanathan, B.; Selvam, P. *Appl. Catal., A* **2009**, *353*, 160−165.

(31) Wang, W.; Yang, Q.; Zhou, R.; Fu, H. Y.; Li, R. X.; Chen, H.; Li, X. J. *J. Organomet. Chem.* **2012**, *697*, 1−5.

(32) So, C. M.; Lau, C. P.; Chan, A. S. C.; Kwong, F. Y. *J. Org. Chem.* **2008**, *73*, 7731−7734.

(33) Okumura, K.; Tomiyama, T.; Okuda, S.; Yoshida, H.; Niwa, M. *J. Catal.* **2010**, *273*, 156−166.

(34) De Vries, A. H. M.; Mulders, J. M. C. A.; Mommers, J. H. M.; Henderickx, H. J. W.; De Vries, J. G. *Org. Lett.* **2003**, *5*, 3285−3288.

(35) Amarnath, K.; Kumar, J.; Reddy, T.; Mahesh, V.; Ayyappan, S. R.; Nellore, J. *Colloids Surf., B* **2012**, *92*, 254−261.

DOI: 10.1021/acs.inorgchem.5b01171
Inorg. Chem. 2015, 54, 9002−9012

(36) Hafiz, A. A.; Negm, N. A.; Elawady, M. Y. *Egypt. J. Chem.* **2004**, *47*, 369−378.
(37) Campanac, C.; Pineau, L.; Payard, A.; Baziard-Mouysset, G.; Roques, C. *Antimicrob. Agents Chemother.* **2002**, *46*, 1469−1474.
(38) Kumar, R. S.; Arunachalam, S. *Biophys. Chem.* **2008**, *136*, 136−144.
(39) Akanni, M. S.; Okoh, E. K.; Burrows, H. D.; Ellis, H. A. *Thermochim. Acta* **1992**, *208*, 1−41.
(40) Manna, A.; Imae, T.; Iida, M.; Hisamatsu, N. *Langmuir* **2001**, *17*, 6000−6004.
(41) Bauer, A. W.; Kirby, W. M.; Sherris, J. C.; Turck, M. *Am. J. Clin. Pathol.* **1966**, *45*, 493−496.
(42) Indu, M. N.; Hatha, A. A. M.; Abirosh, C.; Harsha, U.; Vivekanandan, G. *Braz. J. Microbiol.* **2006**, *37*, 153−155.
(43) Kaur, G.; Karir, G.; Mehta, S. K. *Colloids Surf., A* **2013**, *434*, 25−34.
(44) Kumaraguru, N.; Santhakumar, K. *Polyhedron* **2006**, *25*, 2452−2458.
(45) Orihara, Y.; Matsumura, A.; Saito, Y.; Ogawa, N.; Saji, T.; Yamaguchi, A.; Sakai, H.; Abe, M. *Langmuir* **2001**, *17*, 6072−6076.
(46) Kunitake, T.; Nakashima, N.; Shimomura, M.; Okahata, Y.; Kano, K.; Ogawa, T. *J. Am. Chem. Soc.* **1980**, *102*, 6642−6644.
(47) Griffith, W.; Robinson, S. D.; Swars, K. *Gmelin Handbook of Inorganic Chemistry, Palladium Supplement;* Springer: Berlin, Germany, 1989; (a) 124, (b) 127, (c) 204, (d) 88.
(48) Aizawa, H. *J. Appl. Crystallogr.* **2010**, *43*, 630−631.
(49) Glatter, O. *J. Appl. Crystallogr.* **1980**, *13*, 577−584.
(50) Nimini, P. A.; Babaluo, A. A.; Bayati, B. *Int. J. Nanosci. Nanotechnol.* **2007**, *3*, 37−44.
(51) Petla, R. K.; Vivekanandhan, S.; Misra, M.; Mohanty, A. K.; Satyanarayana, N. *J. Biomater. Nanobiotechnol.* **2012**, *3*, 16695−11.
(52) Wojcieszak, R.; Genet, M. J.; Eloy, P.; Ruiz, P.; Gaigneaux, E. M. *J. Phys. Chem. C* **2010**, *114*, 16677−16684.
(53) Lim, J. K.; Yeap, S. P.; Che, H. X.; Low, S. C. *Nanoscale Res. Lett.* **2013**, *8*, 381−95.
(54) Liao, T. T.; Shi, Y. L.; Jia, J. W.; Wang, L. *Biomed. Environ. Sci.* **2010**, *23*, 219−229.
(55) Zhang, Y. Z.; Zhou, B.; Liu, Y. X.; Zhou, C. X.; Ding, X. L.; Liu, Y. *J. Fluoresc.* **2008**, *18*, 109−118.

DOI: 10.1021/acs.inorgchem.5b01171
Inorg. Chem. 2015, 54, 9002−9012